Dalton Transactions

Accepted Manuscript

ROYAL SOCIETY OF CHEMISTRY

www.rsc.org/dalton

Antisite-disorder, magnetic and thermoelectric properties of Mo-rich $Sr_2Fe_{1-y}Mo_{1+y}O_6$ ($0 \leq y \leq 0.2$) double perovskites

Srinivasa R. Popuri[1], Debbie Redpath[1], Gavin Chan[1], Ronald I. Smith[2], Oscar Cespedes[3], and Jan-Willem G. Bos[1]*

[1]*Institute of Chemical Sciences and Centre for Advanced Energy Storage and Recovery, School of Engineering and Physical Sciences, Heriot-Watt University, Edinburgh, EH14 4AS, United Kingdom. Email: j.w.g.bos@hw.ac.uk*

[2]*ISIS Facility, Rutherford Appleton Laboratory, Harwell Oxford, Didcot, OX11 0QX, UK.*

[3]*School of Physics and Astronomy, University of Leeds, Leeds, LS2 9JT, UK*

Structure analysis using X-ray and neutron powder diffraction and elemental mapping has been used to demonstrate that nominal A-site deficient $Sr_{2-x}FeMoO_{6-\delta}$ ($0 \leq x \leq 0.5$) compositions form as Mo-rich $Sr_2Fe_{1-y}Mo_{1+y}O_6$ ($0 \leq y \leq 0.2$) double perovskites at high temperatures and under reducing atmospheres. These materials show a gradual transition from the Fe and Mo rock salt ordered double perovskite structure to a B-site disordered arrangement. Analysis of the fractions of B-O-B' linkages revealed a gradual increase in the number of Mo-O-Mo linkages at the expense of the ferrimagnetic (FIM) Fe-O-Mo linkages that dominate the y = 0 material. All samples contain about 10-15% antiferromagnetic (AF) Fe-O-Fe linkages, independent of the degree of B-site ordering. The magnetic susceptibility of the y = 0.2 sample is characteristic of a small domain ferrimagnet (T_c ~ 250 K), while room temperature neutron powder diffraction demonstrated the presence of G-type AF ordering linked to the Fe-O-Fe linkages (m_{Fe} = 1.25(7) μ_B). The high temperature thermoelectric properties are characteristic of a metal with a linear temperature dependence of the Seebeck coefficient, S (for all y) and electrical resistivity ρ ($y \geq 0.1$). The largest thermoelectric power factor S^2/ρ = 0.12 mW m^{-1} K^{-1} is observed for Sr_2FeMoO_6 at 1000 K.

Introduction

Thermoelectric modules are widely considered as an important component for a sustainable energy future.[1, 2] Traditionally these devices use p- and n-type semiconductors such as Bi_2Te_3, PbTe and $Si_{1-x}Ge_x$ to convert heat into electricity. The efficiency of a thermoelectric material is given by its figure of merit: $ZT = (S^2/\rho\kappa)T$, where S is the Seebeck coefficient, ρ is the electrical resistivity, κ ($\kappa_{el} + \kappa_{lat}$) is the thermal conductivity (sum of the electronic and lattice thermal conductivities) and T is the absolute temperature. For good thermoelectric performance, materials with a large power factors ($S^2\sigma$) and low κ are needed. Transition metal oxides have only relatively recently been appreciated as promising thermoelectric materials. Their advantageous properties include high-temperature stability , non-toxicity, in many cases low cost, and compatibility with CMOS fabrication techniques.[3, 4] The main disadvantage is that most oxides have poor power factors. This perception changed after the discovery of high $S^2\sigma$ in metallic p-type Na_xCoO_2.[5] Thereafter, several other oxide based materials have been explored such as ZnO,[6, 7] $SrTiO_3$,[8, 9] (misfit) cobaltates,[10-13] and $CaMnO_3$.[14, 15] Despite this considerable research effort, the performance of most of the oxides investigated remains poor compared to the traditional semiconductor materials, and the search for novel efficient oxide materials is ongoing.

The double perovskite Sr_2FeMoO_6 ($A_2BB'O_6$) has been extensively investigated due to its large low field magnetoresistances and spin-polarised conduction.[16] The polarised conduction arises from a double exchange type mechanism where itinerant down-spin Mo^{5+} (t_{2g}^1; S = 1/2) electrons align non-conducting up-spin Fe^{3+} ($t_{2g}^3e_g^2$; S = 5/2) electrons, resulting in a FIM spin structure with a magnetisation of 2(5/2-1/2) = 4 μ_B per formula unit.[16, 17] From a chemical perspective, Sr_2FeMoO_6 can be considered to be in a $Fe^{2+} + Mo^{6+} \leftrightarrow Fe^{3+} + Mo^{5+}$ mixed valence state. The spin-polarisation and magnetoresistance are highly sensitive to Fe and Mo cation inversion,[18-21] which introduces AF Fe-O-Fe and non-magnetic Mo-O-Mo linkages.[17] Recently, Sr_2FeMoO_6 has also attracted some interest for use as a fuel cell cathode.[22] In terms of thermoelectric performance, Sr_2FeMoO_6 is characterised by a low S = -50 $\mu V\ K^{-1}$ at 1073 K. However, this can be increased by partial

replacement of Sr by Ba (S_{1073K} = -125 μV K^{-1}), leading to S^2/ρ values of 0.08 mW m^{-1} K^{-2} (Ref. 23). Measurements of the thermal conductivity showed a 1/T dependence characteristic of a crystalline solid but with a very low κ = 0.2 W m^{-1} K^{-1} at 1073 K, which resulted in ZT = 0.3 at 1073 K. This compares to κ = 6 W m^{-1} K^{-1} at high temperatures for $SrTiO_3$ with only Ti^{4+} as a B-site cation.[24] A note of caution is that the thermal conductivity measurements may have been affected by sample porosity, which is known to lead to significant underestimates of κ. Indeed, follow up studies on the $Sr_{2-x}Ca_xFeMoO_6$ and hole doped $Sr_{2-x}K_xFeMoO_6$ series (sample density 90-95%) gave high-temperature thermal conductivities between 2-4 W m^{-1} K^{-1}.[25, 26] Nevertheless, it is interesting to explore the thermoelectric properties of Sr_2FeMoO_6 based systems further. Recent work from our group and others on A-site deficient $SrTiO_3$ led to the observation of two main effects: glass-like thermal conductivities (linear in T) for large concentrations of vacancies (27%) but also improved electrical conductivities for samples with a relatively low concentration of vacancies (7%).[24, 27-29] For these reasons, we undertook an investigation of nominally A-site deficient $Sr_{2-x}FeMoO_{6-\delta}$ compositions ($0 \le x \le 0.5$), where some oxygen deficiency is required to maintain electrically conducting samples (e.g. for x = 0.5 Fe^{3+} and Mo^{6+} are expected for δ = 0). Our structure analysis demonstrates that the nominal A-site deficiency does not carry over into the final product of the reactions and instead a series of Mo-rich $Sr_2Fe_{1-y}Mo_{1+y}O_6$ double perovskites form.

Experimental

Polycrystalline $Sr_{2-x}FeMoO_6$ (x=0, 0.15, 0.25, 0.35 and 0.5) samples were prepared using standard solid-state chemistry reactions. Stoichiometric amounts of $SrCO_3$, Fe_2O_3 and MoO_3 were mixed using a mortar and pestle, pressed into pellets and heated at 1350°C in 5% H_2 in N_2 for 12 hr. The samples were then ground, re-pressed and sintered at 1400°C in the same atmosphere for 4 hr. The heating and cooling rates were kept at 10 K/min. After the final reaction step, Fe flakes were observed on the surface of the pellets for the samples with x > 0.15. These were scraped off and the

pellets were lightly sanded. Laboratory X-ray powder diffraction (XRD) data were collected on a Bruker D8 Advance diffractometer with Cu $K_{\alpha 1}$ radiation. Room temperature time-of-flight neutron powder diffraction (NPD) data were collected on a 2 gram sample of the x = 0.5 composition on the GEM medium resolution diffractometer at the ISIS pulsed spallation neutron source, Rutherford Appleton Laboratory, UK. A multi-histogram (GEM detector banks 3–6) Rietveld fit to the NPD data was done using the GSAS and EXPGUI suite of programmes.[30, 31] The microstructure was analysed using a Quanta 650 FEG ESEM equipped with an Oxford Instruments X-max 150^N detector for elemental mapping. The working distance, beam spot size and collecting time were 10 mm, 4.5mm and 120 sec respectively. The temperature dependence of the electrical resistivity and Seebeck coefficient were measured using Linseis LSR-3 instrument. The DC magnetic susceptibility (H=10 kOe) was measured using a Quantum Design MPMS vibrating sample magnetometer in the $2 \leq T \leq 400K$ interval.

Results

Composition and Structure: The observation of Fe-flakes on the surface of some of the pellets and in the diffraction patterns (see below) strongly suggested that the composition of our perovskite samples had changed during high-temperature reaction under 5% H_2/N_2 atmosphere. This prompted further investigations using scanning electron microscopy (SEM), energy dispersive X-ray (EDX) elemental analysis and Rietveld analysis of X-ray and neutron powder diffraction data. The EDX measurements were performed on three random spots of ca. 8x9 μm for each sample, and the average values of the atomic ratios were used in the composition calculations. These results are summarized in Table 1 and reveal that a non-A-site deficient and Mo-rich $Sr_2Fe_{1-y}Mo_{1+y}O_6$ series has formed. The experimental compositions are as follows y = 0 (x = 0), 0.04 (x = 0.15), 0.08 (x = 0.25), 0.13 (x = 0.35) and 0.20 (x = 0.5). In order to investigate the sample homogeneity in more detail, large area elemental maps (Sr, Fe and Mo) were collected for the y = 0.2 composition. The results are shown in Fig. 1. This demonstrates that all elements exhibit a homogeneous distribution,

indicating the product is free from macroscopic phase segregation. Some Fe-rich regions corresponding to iron particles are observed in the Fe map.

The room temperature XRD patterns for the $Sr_2Fe_{1-y}Mo_{1+y}O_6$ samples are shown in Fig. 2. The patterns for $0 \leq y \leq 0.13$ can be indexed using the tetragonal I4/m superstructure reported for Sr_2FeMoO_6, which allows for Fe/Mo rocksalt ordering,[32] while the I4/mcm structure with a disordered B-cation arrangement was appropriate for y = 0.2. Both space groups correspond to the $a^0a^0c^-$ Glazer tilt system.[33, 34] A monotonic shift of the diffraction peaks to lower angles is observed and indicates a systematic expansion in the unit cell parameters as y-increases. The insets highlight the evolution of the (101) reflection that is a measure of the degree of Fe and Mo ordering, and the cluster of the (420), (332) and (116) reflections that can be seen to merge for larger y. The reduced (101) intensity signals a gradual loss of B-cation ordering, while the merging of the higher angle reflections shows a reducing tetragonal distortion. In addition to the major phase, there is also evidence for a minor iron impurity phase for $y \geq 0.08$.

Rietveld analysis of the XRD data was used to determine the distribution of the B-cations. These results are summarized in Table 1. Good fits were obtained using the compositions obtained from the elemental analysis with a gradual decrease in B-site ordering observed as the Mo content increases. In these refinements a full occupancy of the oxygen sites was assumed, and the oxygen positions were kept fixed at values reported for Sr_2FeMoO_6 (Ref. 35), and as determined from our neutron powder diffraction analysis on the y = 0.2 sample (see below). The fitted weight fractions of the Fe impurity are 0.54(1), 1.82(7) and 2.39(9) % for y = 0.08, 0.13 and 0.20. The evolution of the lattice parameters is given in Fig. 3. The linear changes in the unit cell parameters with composition were noted in an earlier study and our values are in excellent agreement with those published before.[36, 37] For example, for the c-axis a slope of 0.043Å/y was reported, while our slope is 0.045Å/y. In order to gain insight into the oxygen stoichiometry a 2 gram sample of the y = 0.2 sample was studied using neutron powder diffraction. The final Rietveld fit is shown in Fig. 4 and the refined unit cell and atomic parameters as well as selected bond distances and angles are

summarised in Table 2. The Rietveld fitting confirmed the assignment of the I4/mcm superstructure that was initially made based on X-ray diffraction. The refined composition is $Sr_2Fe_{0.784(2)}Mo_{1.216(2)}O_{5.996(1)}$ signalling a stoichiometric oxygen content, and an overall composition which is in excellent agreement with the EDX and XRD based compositions (Table 1). The observation of weak intensity in the (101) reflection at d ~ 4.55 Å in the neutron diffraction data (GEM Bank 3, Fig. 4) absent in the XRD patterns, indicated the presence of AF order at room temperature. The intensity was successfully fitted assuming a G-type ordering of a simple cubic Fe perovskite sublattice (e.g. as in $LaFeO_3$). The refined magnetic moment was 1.25(7) μ_B and is aligned along the crystallographic c-direction. Similar magnetic order has been observed previously in Fe-rich $Sr_2Fe_{1.33}Mo_{0.67}O_6$ (T_N ~ 250 K) that contains a 1:1 ordering of Fe and ($Mo_{0.67}Fe_{0.33}$),[38] and in highly disordered Sr_2FeMoO_6 (T_N ~ 750 K) with only 18% cation order.[39] Ordered magnetic moments of 1.4 and 2.2 μ_B/Fe atom were reported for these two compositions, respectively.[38, 39]

Magnetic susceptibility: The temperature and field dependences of the magnetisation (M) of the y = 0.2 sample are shown in Figure 5. The field dependence M(H) (inset to Fig. 5) features a small hysteresis and is typical of a soft ferromagnet or a superparamagnet (small domain ferromagnet). This is in keeping with the presence of disrupted FIM Fe-O-Mo patches in this B-site disordered composition. The temperature dependence of the magnetisation M(T) is compared to a sample of similar composition from the literature.[37] A transition is evident at 250 K, in agreement with the literature data. The M(T) data also reveal a substantial ferromagnetic background due to the presence of metallic Fe. A saturation magnetisation of 2 μ_B/f.u (M_{sat} = 25.9 emu/gr) is reported for $Sr_2Fe_{0.8}Mo_{1.2}O_6$ whereas we observed a magnetization value of 37.3 emu/gr. Assuming that the difference is accounted for by elemental Fe (M_{sat} = 221.7 emu/gr),[40] leads to an estimated 5.1 wt% of Fe in our sample. This is in good agreement with the values obtained from Rietveld analysis (Table 1 and 2).

Thermoelectric properties: The temperature dependence of S, ρ and S^2/ρ for the $Sr_2Fe_{1-y}Mo_{1+y}O_6$ samples are shown in Figure 6. The S(T) curves have linear temperature dependences and vary

smoothly with composition (Figure 6a). The linear S(T) is characteristic of a metal and the observed S_{1000K} = -55 μV K^{-1} for Sr_2FeMoO_6 is consistent with earlier reports.[23, 25, 26] The slope of the S(T) curves was used to estimate the carrier concentration using $S = (8\pi k_B^2/3eh^2)m^*(\pi/3n)^{2/3}T$, where k_B is Boltzmann's constant, e is the electronic charge, h is Planck's constant, m^* is the effective mass and n is the carrier concentration.[41] An effective mass of $3.3m_e$ was used in these calculations and the results are summarized in Table 1 and discussed below.[42, 43] The magnitude of S is reduced with increasing Mo content which is consistent with a transition to a metallic system that is also evident from the ρ(T) data. The electrical resistivity for y = 0 decreases from ~ 100 mΩ cm at 300 K to 3 mΩ cm at 1000 K and shows two transitions at ~475 K and ~625 K (Figure 6b). Similar transitions were observed in the earlier report on the $Sr_{2-x}Ba_xFeMoO_6$ series.[23] The origin of these anomalies is not clear but it is worth noting the absence of any transitions in S(T), suggesting that these may be due to extrinsic factors. The y = 0.04 and 0.08 samples contain signatures of these anomalies but for y = 0.13 and 0.20 smoothly varying metallic varying ρ(T) were observed. The latter samples have ρ_{300K} ~ 0.5 mΩ cm increasing to ρ_{1000K} ~ 1 mΩ cm. It is possible that the semiconducting behaviour observed for the lower y values is due to grain boundary effects that are suppressed at higher temperatures and with increased Mo content. The thermoelectric power factors are too small for these materials to be useful thermoelectrics with largest values of 0.11 and 0.04 mW m^{-1} K^{-2} at 1000 K for y = 0 and y = 0.2, respectively (Figure 6c).

Discussion

Elemental and structure analysis demonstrates that the nominal A-site deficient $Sr_{2-x}FeMoO_{6-\delta}$ compositions form a series of Mo-rich non-A-site deficient $Sr_2Fe_{1-y}Mo_{1+y}O_6$ perovskites under high-temperature (1350-1400 °C) and reducing conditions (5% H_2 in N_2). This suggests that these mixed Fe and Mo perovskites do not tolerate A-site and/or oxygen vacancies, at least under the employed synthetic conditions. It may be possible to stabilise the hypothetical $Sr_{0.5}FeMoO_6$ compound with Fe^{3+} and Mo^{6+} using soft chemistry methods and under oxidising atmospheres. This

would, however, involve losing the favourable electronic properties based on the $Fe^{2+/3+}$ and Mo^{5+6+} redox couple,[16] leading to poor semiconducting or electrically insulating behaviour.

The $Sr_2Fe_{1-y}Mo_{1+y}O_6$ materials show a gradual transition from the largely B-site ordered y = 0 composition to the fully disordered y = 0.2 composition. One insightful way to think about these materials is not in terms of Fe/Mo ordering but in terms of the fractions of B-O-B' linkages.[44] This enables a comparison between samples with varying degrees of Fe/Mo ordering. The B-O-B' fractions can be calculated from the refined B-site occupancies (Table 1). For example the largely B-site ordered y = 0 composition has $0.9^2 + 0.1^2 = 0.82$ Fe-O-Mo linkages, $0.1 \times 0.9 = 0.09$ Fe-O-Fe and $0.1 \times 0.9 = 0.09$ Mo-O-Mo linkages, whereas the B-site disordered y = 0.2 sample has $2 \times 0.39 \times 0.61 = 0.48$ Fe-O-Mo linkages, $0.39^2 = 0.15$ Fe-O-Fe and $0.61^2 = 0.37$ Mo-O-Mo linkages. The composition dependence of the fractions of B-O-B' linkages are shown in Figure 7. This reveals a gradual increase in the fraction of Mo-O-Mo linkages, demonstrating that the samples become more like $SrMoO_3$. In fact a linear extrapolation of the c-axis which is not affected by Glazer tilting (shown in the inset to Figure 3) leads to a good agreement with the value reported for cubic $SrMoO_3$.[45] This suggests a gradual change in average B-cation oxidation state as y is increased. Extrapolation of the unit cell volume or a-axis which are affected by changes in the octahedral tilt system leads to an overestimate for $SrMoO_3$. As intuitively expected, the increase in Mo-O-Mo linkages occurs at the expense of the Fe-O-Mo linkages; while an almost constant fraction of Fe-O-Fe linkages (0.1-0.15) are observed. This is somewhat unexpected as a-priori both Fe-O-Mo and Fe-O-Fe linkages could have been broken upon introduction of excess Mo, and suggests there may be an energetic or entropic stabilisation for the Fe-O-Fe linkages. The bottom panel of Figure 7 summarizes the 1000 K thermoelectric property data. This reveals a linear decrease of S, coupled to a decrease in ρ as y is increased, and is consistent with the observed transition to metallic behaviour as the Mo-O-Mo fraction is increased. The calculated charge carrier concentrations increase from 1.5×10^{20} cm^{-3} for y = 0 to 6.5×10^{20} cm^{-3} for y = 0.2 (Table 1). These are almost certainly an underestimate as the Hall carrier concentrations of single crystalline Sr_2FeMoO_6 are reported to be

1.1×10^{22} cm^{-3}.[43] Nevertheless, the trend of an increasing amount of charge carriers with y is clear. The metallic carrier concentrations also preclude the small iron impurities from having a significant impact on the thermoelectric properties, unlike in semiconductors where impurities can lead to substantial changes in carrier concentrations. Computational studies show that the introduction of excess Mo results in the presence of a Mo t_{2g} band at the Fermi level, which leads to the loss of the half-metallic conduction for $y > 0.125$.[36] In other words, the $Sr_2Fe_{1-y}Mo_{1+y}O_6$ samples start to resemble non-magnetic $SrMoO_3$. The maximum power factors are ~ 0.1 mW m^{-1} K^{-1} which leads to an estimated upper limit ZT = 0.05 at 1000 K, using literature data for the thermal conductivity.[25, 26] The magnetic susceptibility and hysteresis for the y = 0.2 sample are in good agreement with the literature, and are typical of a ferrimagnet with small magnetic domains (a superparamagnet). The neutron data indicate G-type AF ordering at room temperature involving the Fe-O-Fe linkages of which there are about 15% in this composition. There is no evidence for long range FIM order coinciding with the AF order but further experiments below 250 K are needed to confirm the short range nature suggested by the susceptibility data. The observation of AF order at room temperature despite the small fraction of Fe-O-Fe linkages (below the percolation limit of 20-25%) suggests that this may be stabilised through Fe-O-Mo-O-Fe interactions,[39] which could be ferromagnetic for Mo^{5+} or AF for non-magnetic Mo^{6+} cations.[46] Evidence for the importance of Mo^{5+} comes from a comparison of the Neel temperatures of the $Sr_2Fe(Fe_{0.33}Mo_{0.67})O_6$ (33% Fe-O-Fe) and disordered Sr_2FeMoO_6 (24% Fe-O-Fe) samples mentioned in the results section. The lowest T_N ~ 250 K is observed for $Sr_2Fe(Fe_{0.33}Mo_{0.67})O_6$ which contains Fe^{3+}/Mo^{6+} while the mixed valence Sr_2FeMoO_6 sample has T_N ~ 750 K, suggesting that the presence of Mo^{5+} is key to observe high Neel temperatures.

The results presented here suggest that these samples combine AF long range order (linked to Fe-O-Fe domains), short range FIM ordering (Fe-O-Mo domains) and itinerant electrons (Fe-O-Mo and Mo-O-Mo domains) all in one material. This may offer possibilities for the tuning and coupling of these properties in a single phase material.

Acknowledgements

We acknowledge the Leverhulme Trust, the UK Engineering and Physical Sciences Research Council (EPSRC) (EP/J000884/1 and EP/K036408/1) and the UK Science and Technology Facilities Council (STFC) for provision of GEM Xpress Access beamtime at ISIS. We would also like to acknowledge Jim Buckman, Institute of Petroleum Engineering, Heriot-Watt University, for his help during collection of the SEM-EDX data.

Table 1: SEM-EDX compositions, space group, lattice parameters, tetragonal distortion, Fe/Mo site occupancies, wt% iron impurities, Rietveld goodness of fit, carrier concentration (n) and percentage densities for the $Sr_2Fe_{1-y}Mo_{1+y}O_6$ ($0 \leq y \leq 0.20$) series.

$Sr_{2-x}Fe_{1-y}Mo_{1+y}O_6$					
Nominal	x=0/y=0	x=0.15/y=0	x=0.25/y=0	x=0.35/y=0	x=0.5/y=0
EDX	x=0/y=0	x=0/y=0.038(3)	x=0/y=0.079(2)	x=0/y=0.126(4)	x=0/y=0.198(3)
S.G	I4/m	I4/m	I4/m	I4/m	I4/mcm
a (Å)	5.5718(5)	5.5765(1)	5.5795(1)	5.5839(1)	5.5922(3)
c (Å)	7.9022(1)	7.9049(3)	7.9078(3)	7.9087(2)	7.9114(4)
1-c/√2a ($x10^{-3}$)	3.0	2.5	2.3	1.7	0.52
V ($Å^3$)	245.32(1)	245.82(1)	246.18(2)	246.59(1)	247.41(1)
Fe/Mo	0.90(1)/0.10(1)	0.84(1)/0.16(1)	0.78(3)/0.22(3)	0.72(3)/0.28(3)	0.39(2)/ 0.61(4)
Mo/Fe	0.90(1)/0.10(1)	0.88(1)/0.12(1)	0.86(3)/0.14(3)	0.85(3)/0.15(3)	
Wt.% Fe	-	-	0.54(1)	1.82(7)	2.39(9)
Reduced χ^2	1.1	1.2	1.3	1.7	1.9
n (cm^{-3})	1.5	2.1	2.5	3.5	6.5
% density	75	89	90	90	85

I4/m: Sr: 4d (1/2, 0, 1/4); Fe/Mo: 2a (0, 0, 0); Mo/Fe: 2b (0, 0, 1/2); O1: 4e (0, 0, 0.252); O2: 8h (0.255, 0.249, 0).
I4/mcm: Sr: 4d (1/2, 0,1/4); Fe/Mo: 4c (0,0,0); O1: 4a (0, 0, 0.25); O2: 8h (0.26, 0.76, 0).

Table 2: Refined crystallographic parameters and selected bond distances and angles for $Sr_2Fe_{0.784(1)}Mo_{1.216(2)}O_{5.996(1)}$ from Rietveld fits against GEM neutron powder diffraction data.

	Wyckoff position	x	y	z	U_{iso} ($Å^2$)	Occupancy
Sr	4d	0	0.5	0.25	0.00892(9)	1
Fe	2a	0	0	0	0.00257(7)	0.392(6)
Mo	2b	0	0	0	0.00257(7)	0.608(6)
O1	4e	0	0	0.25	0.00856(7)	1.002(1)
O2	8h	0.2607(1)	0.7607(2)	0	0.00856(7)	0.998(1)

	Bond distance (Å)		Bond angle (°)
Sr-O1 (x4)	2.854(2)	Mo/Fe-O1-Mo/Fe (x2)	180
Sr-O1 (x4)	2.734(1)	Mo/Fe-O2-Mo/Fe (x4)	175.07(5)
Sr-O2 (x4)	2.792(3)		
Fe/Mo-O2 (x2)	1.976(1)		
Fe/Mo-O1 (x4)	1.976(4)		

Space group: I4/mcm; a=5.5845(3) Å; c=7.9063(7) Å; V=246.57(2) $Å^3$

Fe magnetic moment: $m_x = m_y = 0$, $m_z = 1.25(7)\ \mu_B$

Figure 1: (a) SEM micrograph and (b-d) EDX elemental distributions for the y = 0.2 sample from the $Sr_2Fe_{1-y}Mo_{1+y}O_6$ series.

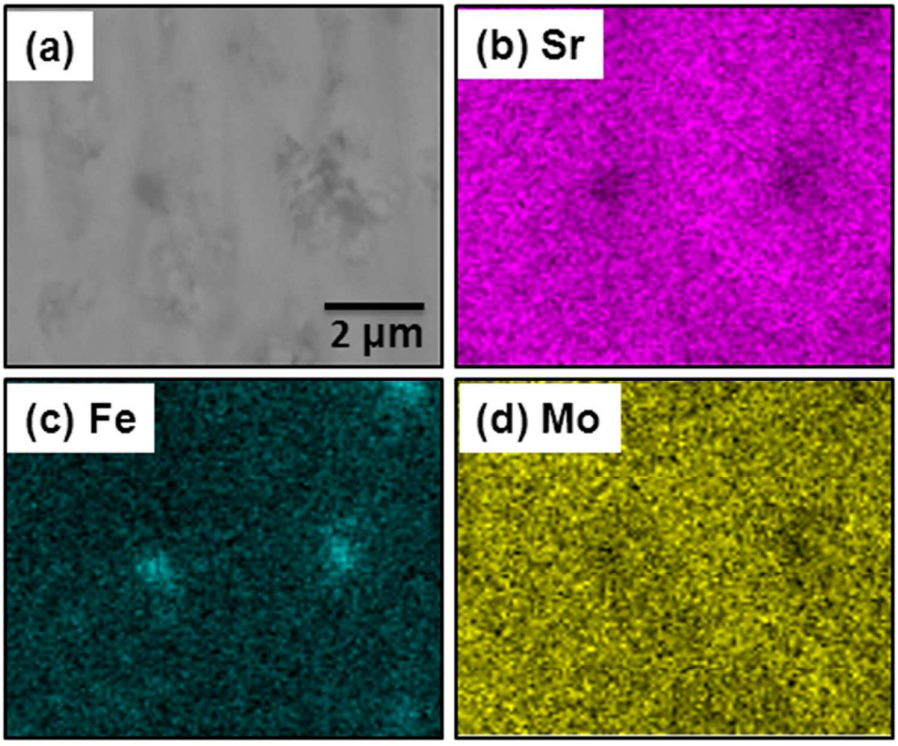

Figure 2: Room temperature X-ray powder diffraction patterns for the $Sr_2Fe_{1-y}Mo_{1+y}O_6$ series. The insets highlight the decreasing intensity of the (101) superstructure reflection indicative of Fe/Mo rocksalt ordering, and the decreasing tetragonal distortion, respectively. The asterisk indicates a small Fe impurity.

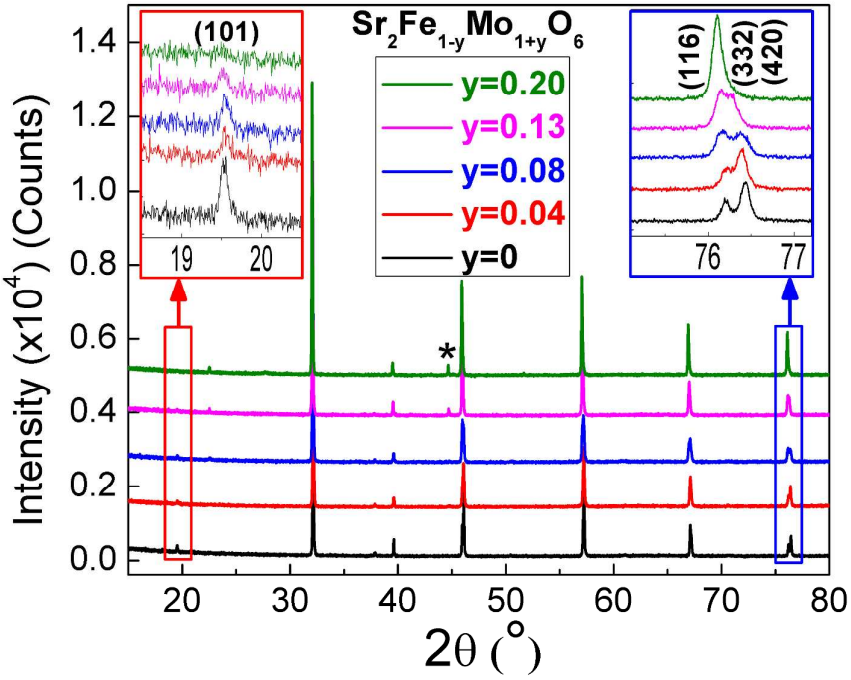

Figure 3: Composition dependence of the lattice parameters for the $Sr_2Fe_{1-y}Mo_{1+y}O_6$ series. The inset shows the interpolation of the lattice parameters up to y = 1, the $SrMoO_3$ lattice parameter was taken from Ref. 45.

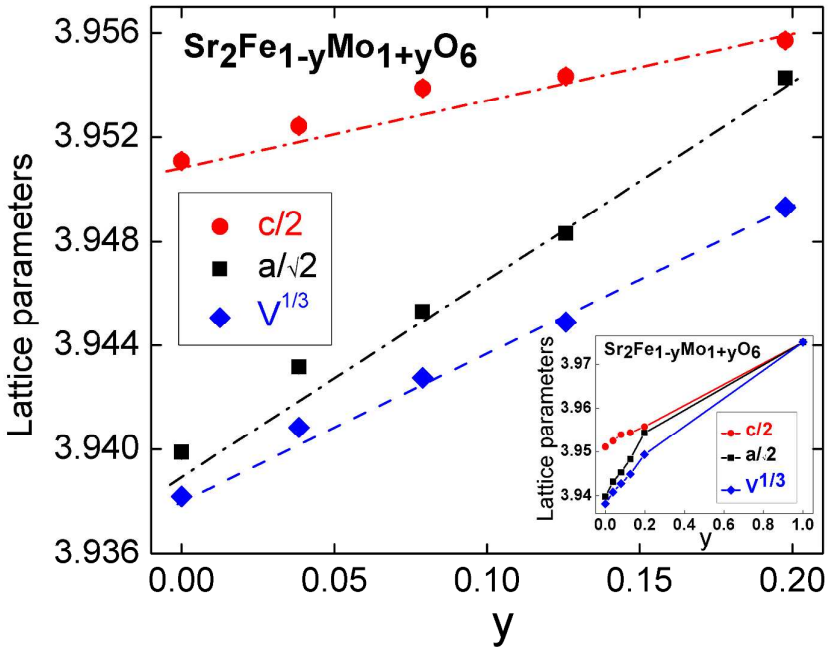

Figure 4: Observed (solid blue circles), calculated (red line) and difference (green line) Rietveld profiles for room temperature neutron powder diffraction data collected on $Sr_2Fe_{0.8}Mo_{1.2}O_6$. Bragg reflection markers correspond to the main phase, nuclear and magnetic contributions, and a 1.5 wt%. Fe impurity (top to bottom). The prominent (101) magnetic reflection is indicated by the green arrow.

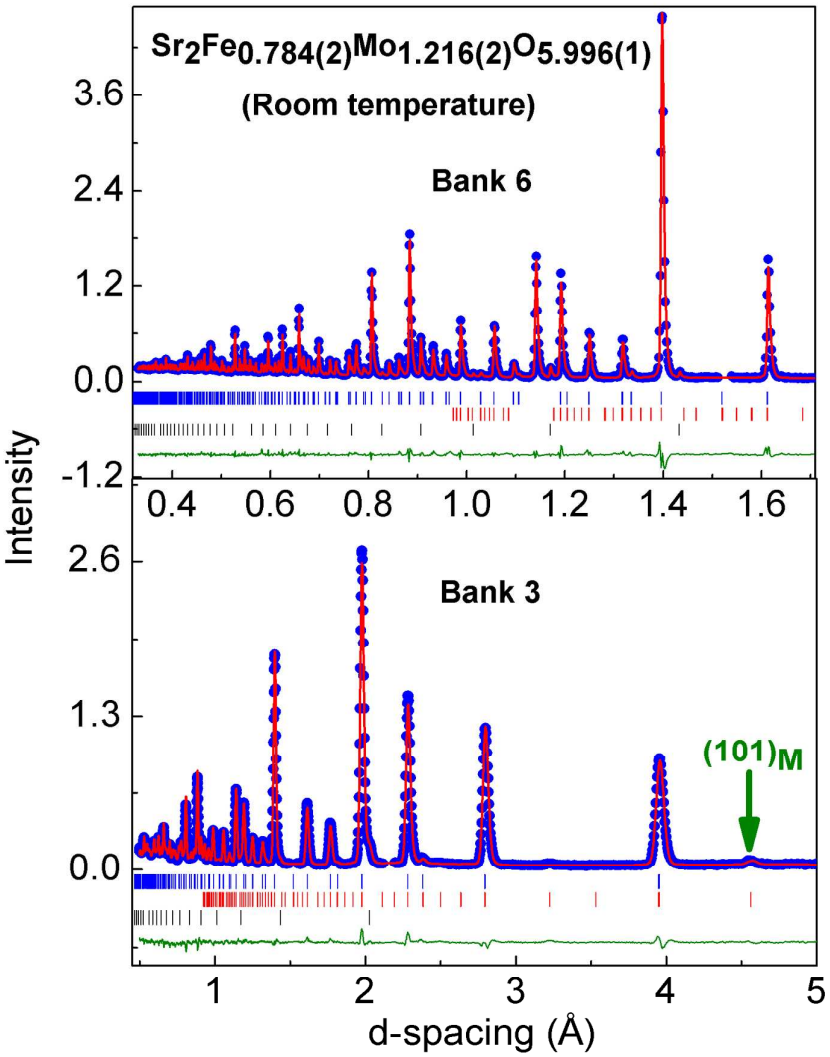

Figure 5. Temperature dependence of the magnetization for $Sr_2Fe_{0.8}Mo_{1.2}O_6$. Data on a sample of similar composition from Ref. 37 is included for comparision. The inset shows the M(H) hysterisis loop at 2K.

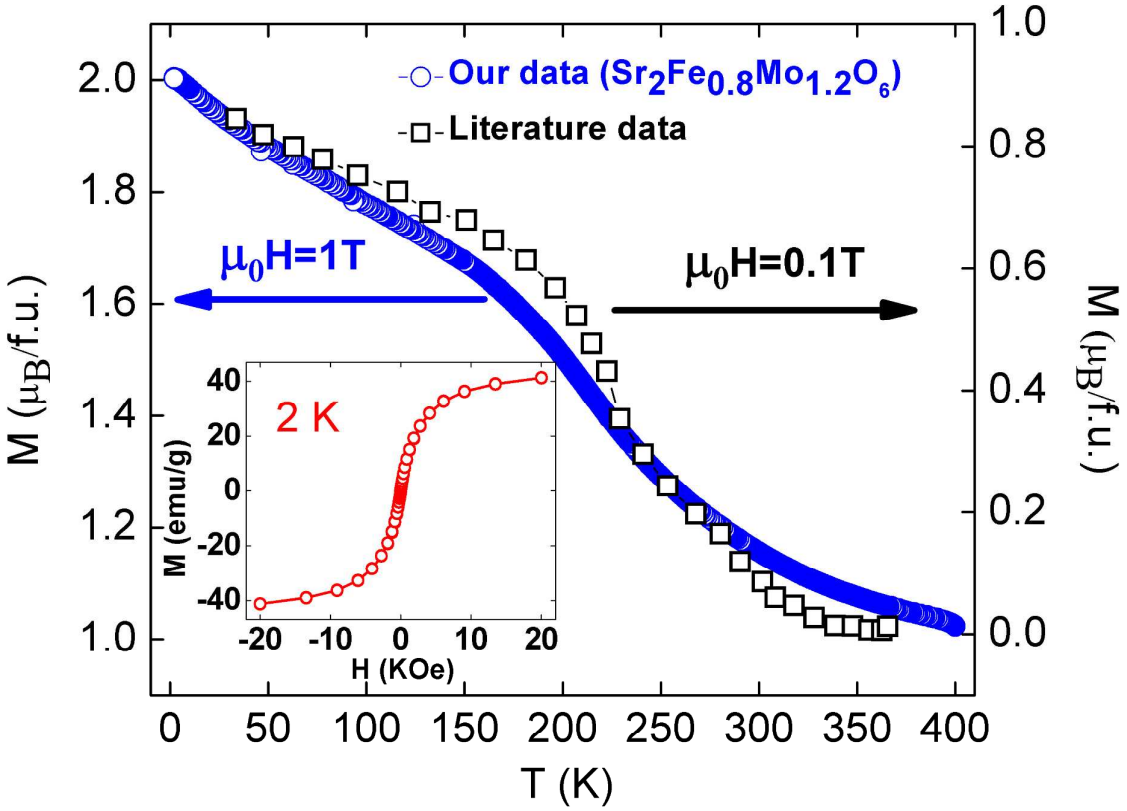

Figure 6: Temperature dependence of (a) the Seebeck coefficient (S), (b) the electrical resistivity (ρ) and (c) the thermoelectric power factor (S^2/ρ) for the $Sr_2Fe_{1-y}Mo_{1+y}O_6$ series.

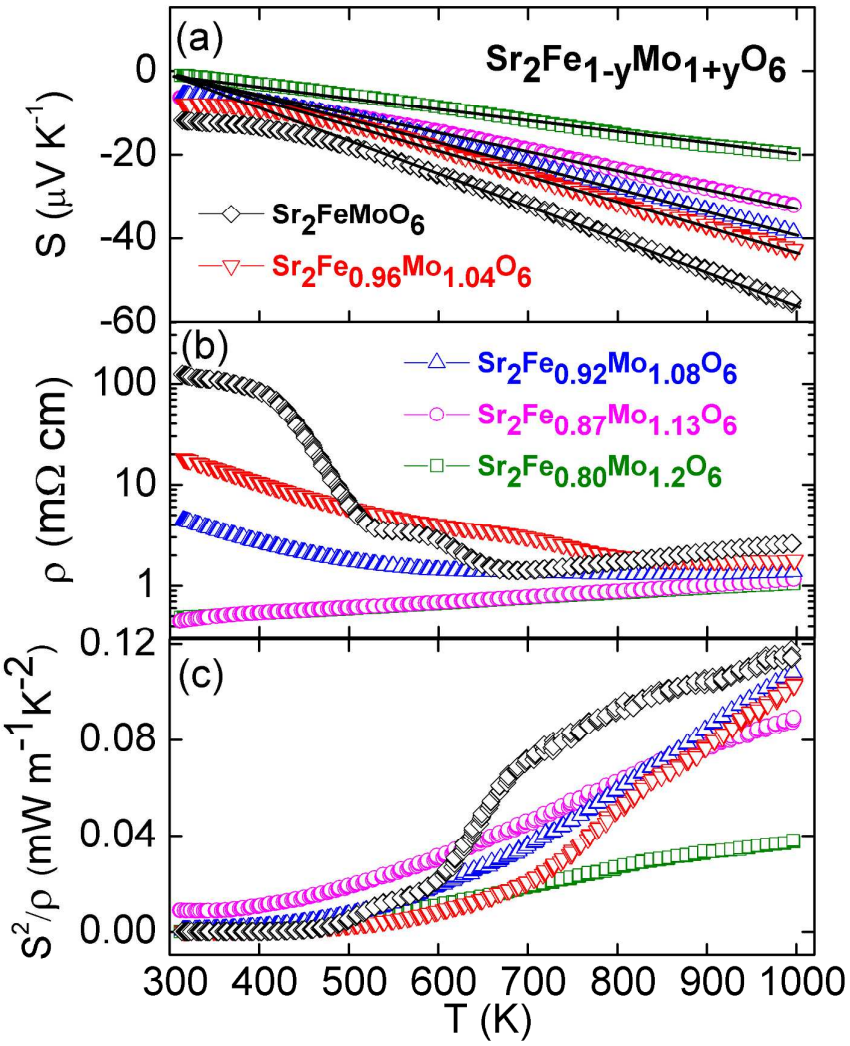

Figure 7: Comparison of (a) the changes in structure quantified using the fraction of B-O-B' linkages and (b) the thermoelectric properties for the $Sr_2Fe_{1-y}Mo_{1+y}O_6$ ($0 \leq y \leq 0.20$) series.

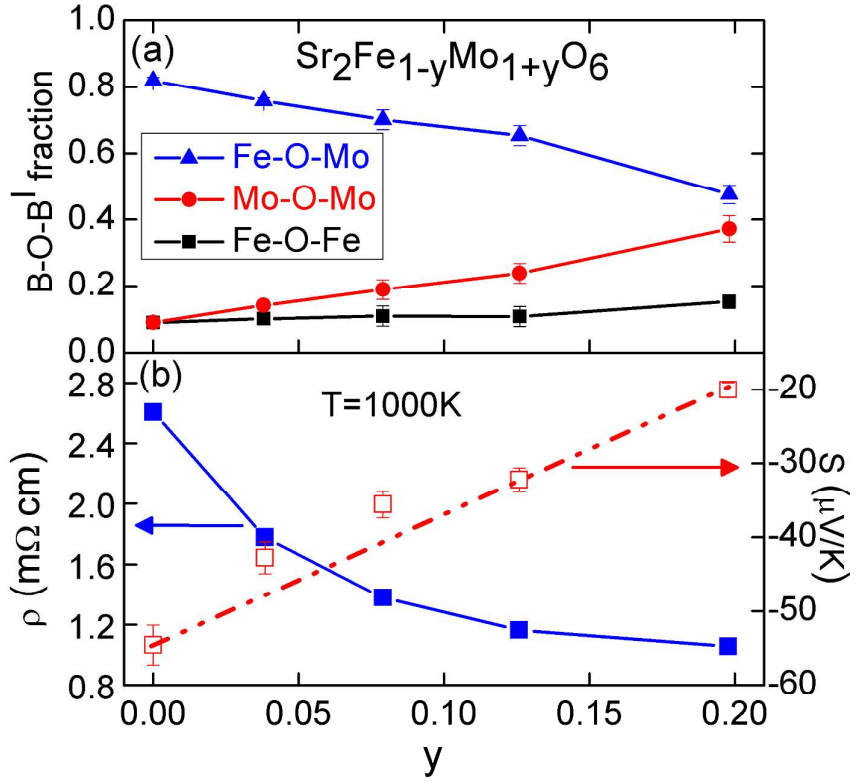

References

1. G. J. Snyder and E. S. Toberer, *Nature Materials*, 2008, **7**, 105-114.
2. D. M. Rowe, ed., *Thermoelectrics Handbook: Macro to Nano*, CRC Press, Boca Raton, 2006.
3. J. W. Fergus, *Journal of the European Ceramic Society*, 2012, **32**, 525-540.
4. J. He, Y. F. Liu and R. Funahashi, *Journal of Materials Research*, 2011, **26**, 1762-1772.
5. I. Terasaki, Y. Sasago and K. Uchinokura, *Physical Review B*, 1997, **56**, 12685-12687.
6. M. Ohtaki, T. Tsubota, K. Eguchi and H. Arai, *Journal of Applied Physics*, 1996, **79**, 1816-1818.
7. T. Tsubota, M. Ohtaki, K. Eguchi and H. Arai, *Journal of Materials Chemistry*, 1997, **7**, 85-90.
8. S. Ohta, T. Nomura, H. Ohta and K. Koumoto, *Journal of Applied Physics*, 2005, **97**, 034106.
9. T. Okuda, K. Nakanishi, S. Miyasaka and Y. Tokura, *Physical Review B*, 2001, **63**, 113104.
10. S. W. Li, R. Funahashi, I. Matsubara, K. Ueno, S. Sodeoka and H. Yamada, *Chemistry of Materials*, 2000, **12**, 2424-2427.
11. Y. Miyazaki, K. Kudo, M. Akoshima, Y. Ono, Y. Koike and T. Kajitani, *Japanese Journal of Applied Physics Part 2-Letters*, 2000, **39**, L531-L533.
12. M. Shikano and R. Funahashi, *Applied Physics Letters*, 2003, **82**, 1851-1853.
13. J. W. G. Bos, J. T. Hertz, E. Morosan and R. J. Cava, *Journal of Solid State Chemistry*, 2007, **180**, 3211-3217.
14. D. Flahaut, T. Mihara, R. Funahashi, N. Nabeshima, K. Lee, H. Ohta and K. Koumoto, *Journal of Applied Physics*, 2006, **100**, 084911.
15. M. Ohtaki, H. Koga, T. Tokunaga, K. Eguchi and H. Arai, *Journal of Solid State Chemistry*, 1995, **120**, 105-111.
16. K. L. Kobayashi, T. Kimura, H. Sawada, K. Terakura and Y. Tokura, *Nature*, 1998, **395**, 677-680.
17. D. Serrate, J. M. De Teresa and M. R. Ibarra, *Journal of Physics-Condensed Matter*, 2007, **19**, 023201.
18. A. S. Ogale, S. B. Ogale, R. Ramesh and T. Venkatesan, *Applied Physics Letters*, 1999, **75**, 537-539.
19. L. Balcells, J. Navarro, M. Bibes, A. Roig, B. Martinez and J. Fontcuberta, *Applied Physics Letters*, 2001, **78**, 781-783.
20. M. Garcia-Hernandez, J. L. Martinez, M. J. Martinez-Lope, M. T. Casais and J. A. Alonso, *Physical Review Letters*, 2001, **86**, 2443-2446.
21. J. Navarro, J. Nogues, J. S. Munoz and J. Fontcuberta, *Physical Review B*, 2003, **67**, 174416.
22. A. B. Munoz-Garcia, M. Pavone and E. A. Carter, *Chemistry of Materials*, 2011, **23**, 4525-4536.
23. T. Sugahara, M. Ohtaki and T. Souma, *Journal of the Ceramic Society of Japan*, 2008, **116**, 1278-1282.
24. S. R. Popuri, A. J. M. Scott, R. A. Downie, M. A. Hall, E. Suard, R. Decourt, M. Pollet and J. W. G. Bos, *RSC Advances*, 2014, **4**, 33720-33723.
25. T. Sugahara, T. Araki, M. Ohtaki and K. Suganuma, *Journal of the Ceramic Society of Japan*, 2012, **120**, 211-216.
26. T. Sugahara, N. V. Nong and M. Ohtakic, *Materials Chemistry and Physics*, 2012, **133**, 630-634.
27. A. V. Kovalevsky, A. A. Yaremchenko, S. Populoh, A. Weidenkaff and J. R. Frade, *Journal of Physical Chemistry C*, 2014, **118**, 4596-4606.

28. M. T. Buscaglia, F. Maglia, U. Anselmi-Tamburini, D. Marre, I. Pallecchi, A. Ianculescu, G. Canu, M. Viviani, M. Fabrizio and V. Buscaglia, *Journal of the European Ceramic Society*, 2014, **34**, 307-316.
29. S. S. Jackson, F. Azough and R. Freer, *Journal of Electronic Materials*, 2014, **43**, 2331-2336.
30. A. C. Larson and R. B. Von Dreele, *Los Alamos National Laboratory Report LAUR 86-748*, 2000.
31. B. H. Toby, *Journal of Applied Crystallography*, 2001, **34**, 210-213.
32. M. T. Anderson, K. B. Greenwood, G. A. Taylor and K. R. Poeppelmeier, *Progress in Solid State Chemistry*, 1993, **22**, 197-233.
33. C. J. Howard, B. J. Kennedy and P. M. Woodward, *Acta Crystallographica Section B-Structural Science*, 2003, **59**, 463-471.
34. P. M. Woodward, *Acta Crystallographica Section B-Structural Science*, 1997, **53**, 32-43.
35. O. Chmaissem, R. Kruk, B. Dabrowski, D. E. Brown, X. Xiong, S. Kolesnik, J. D. Jorgensen and C. W. Kimball, *Physical Review B*, 2000, **62**, 14197-14206.
36. R. Mishra, O. D. Restrepo, P. M. Woodward and W. Windl, *Chemistry of Materials*, 2010, **22**, 6092-6102.
37. D. Topwal, D. D. Sarma, H. Kato, Y. Tokura and M. Avignon, *Physical Review B*, 2006, **73**, 094419.
38. M. C. Viola, J. A. Alonso, J. C. Pedregosa and R. E. Carbonio, *European Journal of Inorganic Chemistry*, 2005, 1559-1564.
39. D. Sanchez, J. A. Alonso, M. G. Hernandez, M. J. Martinez-Lope, J. L. Martinez and A. Mellergard, *Physical Review B*, 2002, **65**, 104426.
40. J. Crangle and G. M. Goodman, *Proceedings of the Royal Society of London Series a-Mathematical and Physical Sciences*, 1971, **321**, 477.
41. M. Cutler, J. F. Leavy and R. L. Fitzpatrick, *Physical Review*, 1964, **133**, 1143.
42. H. Yanagihara, W. Cheong, M. B. Salamon, S. Xu and Y. Moritomo, *Physical Review B*, 2002, **65**, 092411.
43. Y. Tomioka, T. Okuda, Y. Okimoto, R. Kumai, K. I. Kobayashi and Y. Tokura, *Physical Review B*, 2000, **61**, 422-427.
44. J. A. Rodgers, A. J. Williams, A. J. Martinez-Lope, J. A. Alonso and J. P. Attfield, *Chemistry of Materials*, 2008, **20**, 4797-4799.
45. R. B. Macquart, B. J. Kennedy and M. Avdeev, *Journal of Solid State Chemistry*, 2010, **183**, 250-255.
46. J. W. G. Bos and J. P. Attfield, *Physical Review B*, 2004, **70**, 174434.

Graphical Abstract

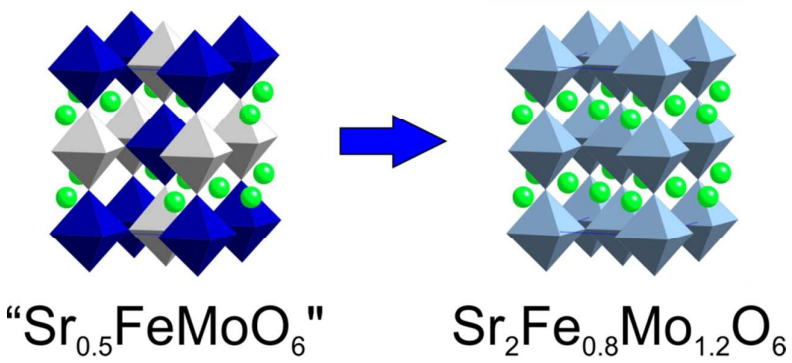

A-site deficiency does not survive in $Sr_{2-x}FeMoO_6$ and instead Mo-rich $Sr_2Fe_{1-y}Mo_{1+y}O_6$ perovskites, characterised by the gradual disordering of Fe and Mo, form.